Manufacturing and characterization of smart composite filaments for additive manufacturing

L.I. Mondragón-Herrera[1*], M.A. Rivero-Ayala[1], A. Balam[1], H. Aguilar-Bolados[2], C. Velasco-Santos[3] and F. Avilés[1]

[1] Unidad de Materiales, Centro de Investigación Científica de Yucatán, Calle 43 No.130 x 32 y 34, Col. Chuburná de Hidalgo, 97205 Mérida, Yucatán, México
[2] Departamento de Polímeros, Facultad de Ciencias Químicas, Universidad de Concepción, Concepción, 3349001, Chile
[3] División de Estudios de Posgrado e Investigación, Tecnológico Nacional de México campus Querétaro, Av. Tecnológico s/n esq. Gral. Mariano Escobedo. Col. Centro Histórico, 76000 Querétaro, Querétaro, México.
* *Corresponding author (luis.mondragon@estudiantes.cicy.mx)*

Keywords: *carbon nanotube composites, conductive polymer filaments, electromechanical response, fused deposition modeling.*

Abstract

Electroconductive polymer nanocomposites processed by fused deposition modeling (FDM) offer a promising route for integrating sensing and actuation functionalities into structural components. However, the relationship between filament properties and the performance of printed structures remains insufficiently understood. Carbon nanotube (CNT) reinforced polymer filaments based on polylactic acid (PLA) and PLA-polyhydroxyalkanoates (PLA–PHA) were fabricated via melt blending and extrusion, and their mechanical, electrical, and piezoresistive responses were compared with those of FDM-manufactured single-layer structures. The incorporation of CNTs to filaments increased stiffness with minimal effect on strength, while FDM processing reduced ductility. Filament electrical conductivity decreased by up to three orders of magnitude after FDM, indicating disruption of the conductive network. In contrast, piezoresistive sensitivity increased after FDM, with gage factors nearly doubling. These results indicate that the FDM process greatly modifies the electrical conductivity and electromechanical sensitivity. The findings establish the filament's electromechanical properties as key design parameter for controlling structure–property relationships governing self-sensing and actuation in FDM-manufactured nanocomposite parts.

1. Introduction

Fused deposition modeling (FDM), also known as fused filament fabrication, is one of the most widely adopted additive manufacturing techniques due to its design flexibility, cost-effectiveness, and capability to fabricate complex geometries with minimal post-processing [1,2]. In recent years, the development of electrically conductive polymer composites for FDM has attracted significant attention, as it enables the integration of structural and functional properties, such as sensing and actuation, within lightweight and customizable components [2]. Conductive filaments are typically produced by incorporating carbon-based nanofillers, such as carbon black, carbon nanotubes (CNTs), or graphenic sheets, into thermoplastic matrices including polylactic acid (PLA), thermoplastic polyurethane (TPU), and acrylonitrile butadiene styrene [3–5]. Among these, PLA and PLA–polyhydroxyalkanoates (PLA–PHA) blends are particularly attractive due to their processability and tunable mechanical performance. Electrical conductivity arises when the filler content exceeds the percolation threshold, forming an interconnected network that enables electron transport. The FDM process itself introduces microstructural features, such as raster orientation, inter-filament interfaces, and porosity, which strongly influence electrical and electromechanical behavior of the FDM-manufactured parts [6,7]. Experimental studies have shown that CNT/PLA filaments can reach conductivities on the order of ~10 S/m or higher at optimized loadings, while highly filled systems may achieve values up to ~10^2 S/m [5,8]. The reported gage factor (GF) for CNT-based FDM composites range from ~1–10 for densely interconnected networks to values exceeding 40–150 in systems dominated by tunneling mechanisms and strain-induced network rearrangement [19,20]. Previous studies have shown a wide range of electromechanical responses for CNT-based composites processed by FDM, highlighting the strong dependence on formulation and processing parameters [19,20]. However, most investigations have focused on printed components, while the intrinsic properties of the precursor filaments remain poorly understood. The correlation between the GF of the precursor filament and its FDM-manufactured part is yet unknown. This is a critical knowledge gap, as filament characteristics, such as filler dispersion, electrical conductivity, and mechanical behavior, directly govern the microstructure and performance of FDM-manufactured specimens. Therefore, the extent to which filament-level properties are preserved, degraded, or even enhanced after FDM processing remains unclear. In this work, CNT-based PLA and PLA–PHA nanocomposite filaments were fabricated via melt blending and single-screw extrusion. Their thermal, mechanical, electrical, and piezoresistive properties are characterized and compared with those of their FDM-manufactured single layer specimens. The actuation capabilities were explored using a multimaterial configuration designed to promote heating through the Joule effect. The results provide insights into the influence of filament-to-FDM structural transformation on conductive network integrity and contribute to understanding the structure–property relationships relevant to the design of self-sensing and actuation systems fabricated by FDM.

2. Materials and methodology

2.1. Materials

Two polymeric matrices were used, corresponding to commercial filaments with a nominal diameter of 1.75 mm made of PLA [9] and a PLA–PHA [10]. Both materials were supplied by colorFabb (Limburg, The Netherlands). Prior to processing, the filaments were pelletized to facilitate compounding. Multiwall CNTs were acquired from Cheap Tubes Inc. (Vermont, USA). The CNTs had an inner diameter of 5–10 nm, an outer diameter of 30–50 nm, and lengths ranging from 1 to 6 µm, with an average length of 2.6 µm [11]. The carbon fibers (TR30S) used for the actuation experiments were commercially sourced from Mitsubishi Rayon Carbon Fiber and Composites Inc. (CA, USA). The material was supplied as a 200 g/m^2 2×2 twill weave fabric, consisting of tows with 3000 filaments, an average filament diameter of approximately 7 µm, and a fiber density of 1.79 g/cm^3. Individual fiber tows were carefully separated from the woven fabric for subsequent use as a heating element. The TPU filament used for actuation was supplied by ColorPlus (Querétaro, Mexico).

2.2. Filament fabrication

The fabrication of both polymeric and nanocomposite filaments involved a multistep process, starting from blending material components and finalizing in filament winding, as illustrated in Figure 1. Initially, polymer (either PLA or PLA-PHA) pellets were dried at 50 °C for 24 h to remove residual moisture. Subsequently, polymer pellets and CNTs were compounded in a three-piece batch mixer. The resulting polymer and composites (0, 2, 4 and 6 wt. % CNTs) were ground (~ mm-diameter particles) using a Brabender mill and subjected to a second drying step at 50 °C for 24 h. The filament was manufactured using a system composed of three main sections, viz., extrusion, cooling, and winding, yielding filaments with diameter 1.68 ± 0.08 mm. Samples were designated according to the CNT concentration followed by the polymer matrix, where the numerical prefix indicates the filler content in wt.%.

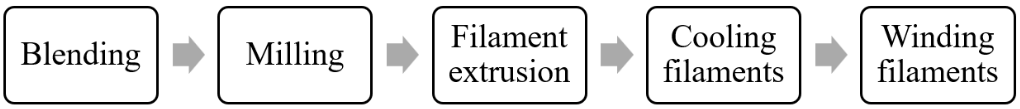

Figure 1. Fabrication process of the polymer and nanocomposite filaments.

2.3. Fused deposition modeling of specimens

To isolate the intrinsic mechanical behavior of the material, single-layer printed structures were employed. FDM-manufactured single-layer specimens were fabricated using a Creality Ender 3 S1 Pro 3D printer (Shenzhen, China). The printing parameters included a nozzle temperature of 200 °C, a nozzle diameter of 0.4 mm, a bed temperature of 60 °C, a layer thickness of 0.3 mm, and a printing speed of 90 mm/s. Type IV specimens for each composition, in accordance with ASTM D638 [12], were produced with the deposition path aligned along the loading direction (0°). Additionally, for electrical resistance measurements, single-layer and unidirectional circular films with a diameter of 5.5 cm were fabricated for each material.

2.4. Morphological analysis of filaments

Scanning electron microscopy (SEM) was used to characterize the surfaces of the filaments. The analysis was carried out with a JEOL JSM-6360LV microscope (Tokyo, Japan) operated at an accelerating voltage of 20 kV under vacuum conditions, coating the specimens with a thin gold layer (~ 20 nm).

2.5. Tensile testing

Tensile tests of the filaments and FDM-manufactured specimens were carried out using a Shimadzu AGS-X universal testing machine equipped with a 1 kN load cell. For each material, ten replicates were tested. The filaments had a total length of 120 mm, with 30 mm at each end used for gripping, resulting in an effective gage length of 60 mm. For the polymer and nanocomposite FDM-manufactured specimens, a crosshead displacement rate of 2 mm/min was applied until failure. A total of ten specimens, fabricated as described in Section 2.3, were tested using a gage length of 38.4 mm. The elastic modulus for both filaments and FDM-manufactured specimens was determined from a linear regression of the stress–strain curve within the strain range of 0.2 % to 1.2 %.

2.6. Electrical resistance measurement

Five segments of each polymer and nanocomposite filaments with length of 30 mm were evaluated for electrical resistance. Copper wires were attached to both ends of each segment using conductive paint and connected to a Keithley 6517B electrometer. The electrical conductivity (σ_e) was determined from the measured resistance (R) at an applied voltage of 20 V as,

$$\sigma_e = \frac{L}{R \cdot A} \quad (1)$$

where A is the cross-sectional area, and L is the filament length. Electrical resistance measurements of FDM-manufactured specimens were conducted using a Keithley 6517B electrometer and a Model 8009 resistivity test fixture (Keithley Instruments). Five circular specimens were fabricated from each material as described in Section 2.3. An alternating polarity method was used at 100 V, reversing polarity every 10 s.

2.7. Piezoresistivity

The piezoresistive response of the nanocomposite filaments and FDM-manufactured specimens under tensile loading was evaluated using the same equipment and testing parameters described in Section 2.5. The distance between the copper electrodes bonded to the filament and FDM-manufactured specimens using conductive paint was fixed at 30 mm. The total length of the tested filament segments was 120 mm. During testing, electrical resistance was measured simultaneously with load and strain. The instantaneous resistance of the filaments was recorded at each load/strain level using a two-probe configuration connected to a benchtop digital multimeter (Agilent DMM 34411A, Santa Clara, USA) with 6½-digit resolution. The relative change in electrical resistance ($\Delta R/R_0$), where R_0 corresponds to the initial resistance prior to deformation, was plotted as a function of strain (ε). The piezoresistive sensitivity was quantified through the gage factor (GF), defined as the slope of the $\Delta R/R_0$ versus ε curve within the linear strain regions [13]. Ten segments of each nanocomposite filament and same number of FDM-manufactured specimen were analyzed.

2.8. Bending actuation tests

For actuation, five rectangular specimens were fabricated by FDM using the equipment and processing parameters described in Section 2.3. Specimens measured 80 mm in length and 5 mm in width. A multilayer architecture was designed to promote electrothermal bending actuation driven by mismatch in the coefficient of thermal expansion. First, a base layer (0.1 mm) of 4CNT/PLA composite was deposited. Subsequently, a carbon fiber tow was manually placed and aligned along the specimen longitudinal axis. Finally, a top layer (0.2 mm) of TPU was printed at a nozzle temperature of 215 °C to encapsulate the fiber and complete the composite structure. All other printing parameters were maintained identical to those previously employed for PLA. For testing, the specimens were rigidly fixed onto a metallic base, forming a cantilever beam setup as shown in Figure 2. Electrical contacts were established by applying conductive paint at both ends of the exposed carbon fiber tow, followed by the attachment of copper wires acting as electrodes.

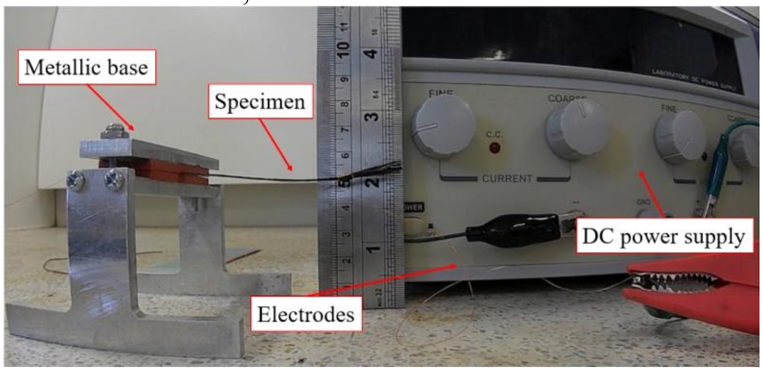

Figure 2. Experimental electrothermal actuation setup.

A constant current of 220 mA was supplied using a DC power source (Matrix MPS-6005L-1, Shenzhen, China). The electrically induced deflection was recorded in real time during actuation using a digital camera and subsequent image analysis. The tip displacement of each specimen was quantified using digital image analysis (ImageJ software, National Institute of Health, Montgomery, USA).

3. Results

3.1. Morphology

Figure 3 shows representative SEM micrographs of the filament cross-sections, including the overall morphology and magnified views of the central (green box) and edge regions (brown box) for PLA, 2CNT/PLA, PLA–PHA, and 2CNT/PLA–PHA. For both polymer matrices, CNTs are well distributed across the cross-section, with no evidence of preferential agglomeration. Filaments containing 4 and 6 wt.% CNT loadings (not shown) exhibit similar dispersion. These results suggest a high degree of homogeneity and confirm the effectiveness of the extrusion and melt-mixing processes in promoting CNT dispersion.

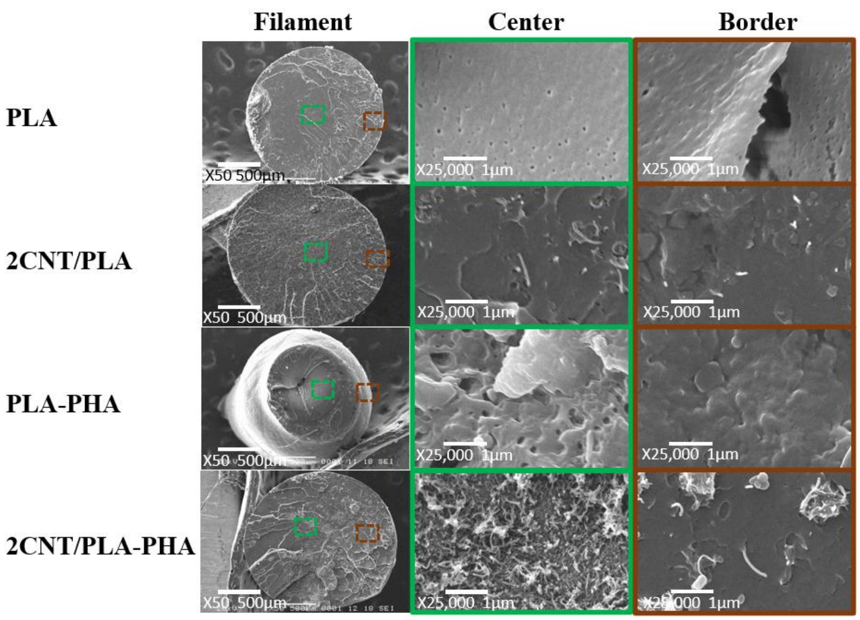

Figure 3. SEM micrographs of polymeric filaments and filaments containing 2 wt.% CNTs (left), together with higher-magnification images of the central (middle) and peripheral regions (right).

3.2. Tensile response

Figure 4a shows the tensile stress (σ) – strain curves of the neat polymers, 4 wt.% CNT filaments and 4 wt.% FDM-manufactured specimens. Figure 4b presents a comparison of the tensile properties of all filaments as a function of CNT concentration. In PLA-based filaments, the elastic modulus (E) showed an increasing trend with CNT content, reaching 2.62 GPa for 6CNT/PLA. Tensile strength (σ_{max}) remained essentially constant (~ 52–54 MPa), while elongation at break (ε_{ult}) slightly decreased with increasing CNT content. These results suggest that, although CNT incorporation may contribute to stiffness enhancement, its effect on strength is limited, likely due to nanotube agglomeration and localized stress concentrations at higher loadings. A similar behavior was observed for PLA–PHA-based filaments, where the elastic modulus increased up to 3.56 GPa for 6CNT/PLA–PHA, but without statistically significant differences among compositions, indicating that the matrix properties dominate the mechanical response.

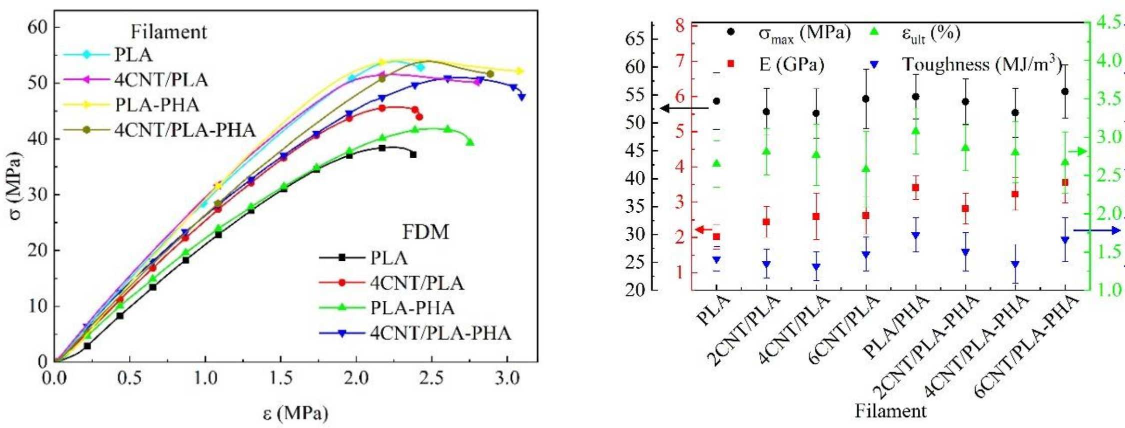

(a) (b)

Figure 4. Mechanical response of polymer filaments and filaments containing 4 wt.% of CNTs. a) Stress–strain response of filaments and corresponding printed specimens, b) comparison of mechanical properties, including elastic modulus, tensile strength, elongation at break, and toughness.

Compared to filaments, all FDM-manufactured specimens exhibited reduced tensile strength and, in most cases, modified toughness. For instance, neat PLA showed a decrease in tensile strength from 53.9 MPa (filament) to 38.5 MPa (FDM). The mechanical properties of FDM-manufactured parts decreased, particularly, the tensile strength decreased by ~ 30% compared to their filament counterparts. This suggest that structural and processing parameters, such as raster orientation, interfacial bonding, void distribution, porosity, and process-induced anisotropy, play an important role alongside intrinsic material properties [7,13–16].

In PLA-based FDM-manufactured specimens, CNT addition led to moderate increases in stiffness, reaching 2.84 GPa for 6CNT/PLA. Tensile strength remained lower than that of the corresponding filaments and did not show a monotonic trend. This behavior indicates that the mechanical performance of FDM structures is governed primarily by interfacial adhesion between deposited roads rather than by the intrinsic properties of the precursor nanocomposite filament. In contrast, PLA–PHA-based FDM-manufactured specimens (not shown) exhibited a more pronounced increase in toughness and strength upon CNT incorporation, with 4CNT/PLA–PHA showing the highest toughness (1.04 MJ/m³). This enhancement is attributed to the multiphase nature of the blend, which promotes improved stress redistribution and energy dissipation mechanisms. However, at higher CNT loadings (6 wt.%), partial agglomeration limits further improvements.

3.3. Electrical conductivity

The electrical conductivity of the polymer and nanocomposite filaments and FDM-manufactured specimen as a function of CNT content are presented in Figures 5a and 5b. The increase in CNT content progressively enhanced conductivity, with increasing to ~10^{-6} S/cm for 4 wt.% and 10^{-3} Ω at 6 wt.%. This trend is associated with the progressive densification and enhanced interconnectivity of the three-dimensional CNT conductive network as filler content increases.

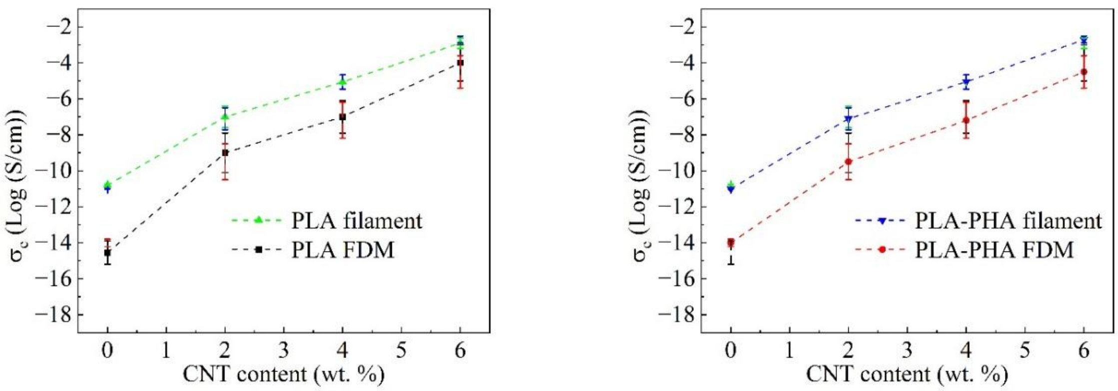

(a) (b)

Figure 5. Electrical conductivity as a function of CNT concentration. a) Filaments, b) FDM-manufactured specimens.

FDM-manufactured specimens exhibited a reduction in conductivity by two to four orders of magnitude compared to filaments. This decrease is primarily associated with the layered architecture inherent to FDM, where inter-strand voids, porosity, and interfacial contact resistance disrupt conductive pathways [15]. Additionally, strand swelling and partial CNT encapsulation during extrusion further hinder interparticle connectivity [17]. Similar observations have been reported in the literature, where filaments exhibit higher conductivity than their printed counterparts [18].

3.4. Piezoresistivity response

The piezoresistive response curves of the filaments and FDM-manufactured specimens with 4 and 6 wt.% CNTs are presented in Figure 6a and 6b, respectively. The corresponding GF values, calculated from the $\Delta R/R_0$–ε curves within the 0.2–1.2 % strain range, are shown in Figure 6c. The piezoresistive characterization results exhibit relatively high scattered values (up to ~30% coefficient of variation), likely associated with variations in CNT dispersion, and agglomeration. As observed for both PLA and PLA–PHA matrices, in general, it has been reported that a reduction in CNT content led to an increase in GF. This is because at high filler loadings, the densely interconnected network reduces the impact of individual pathway disruptions on the electrical resistance [19]. PLA–PHA-based nanocomposites consistently exhibited higher GFs than their PLA counterparts. This is likely due to increased matrix deformability provided by PHA. This behavior aligns with previous studies, where GFs for carbon-based nanocomposites typically range from a few units to several tens, depending on filler content and processing conditions [6,20].

Compared to filaments, FDM-manufactured specimens exhibit higher GFs, approximately doubling in most cases. This indicates that the printing process enhances piezoresistive sensitivity, likely due to architectural and microstructural features such as road interfaces and porosity which could amplify resistance changes under strain. The high GF measured highlights their potential for sensing applications. However, the electromechanical response remains highly dependent on strain range, network morphology, and processing parameters, especially FDM-induced microstructural features.

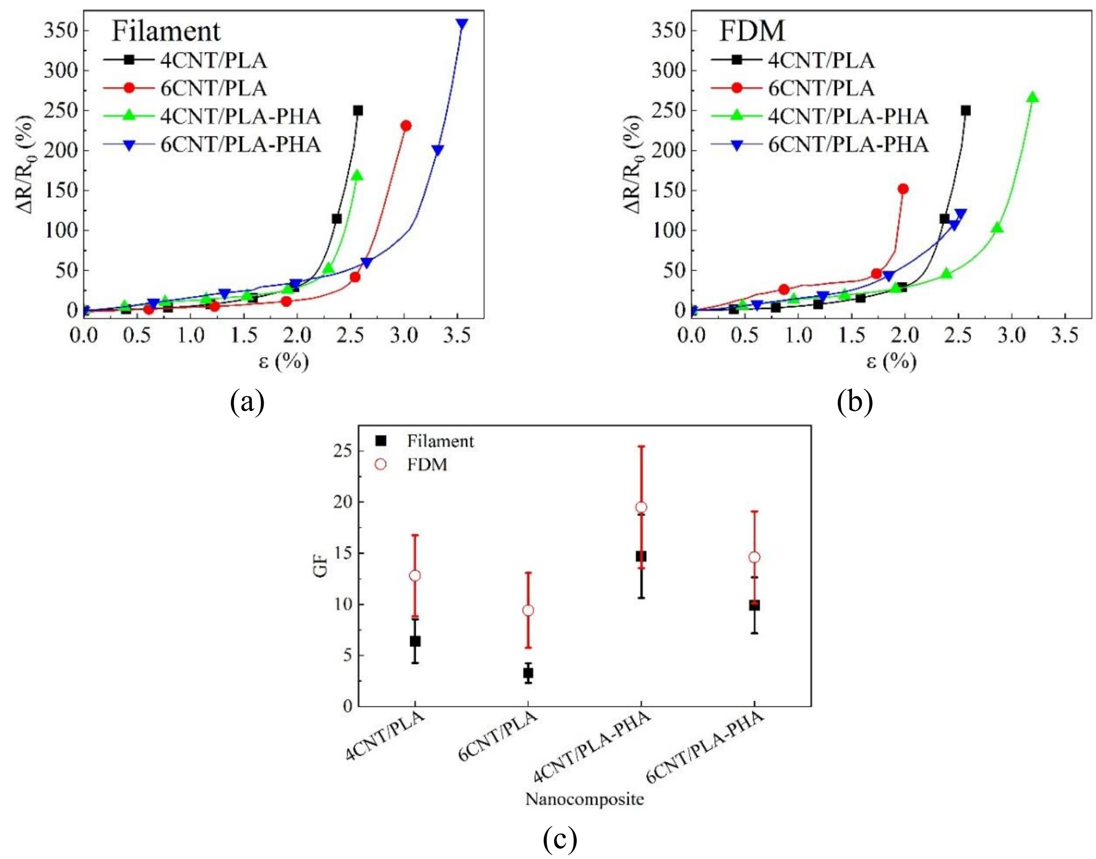

Figure 6. Electromechanical response of nanocomposites. a) $\Delta R/R_0 - \varepsilon$ curves of filaments, (b) $\Delta R/R_0 - \varepsilon$ curves of FDM-manufactured specimens, c) GF for filaments and FDM-manufactured specimens.

3.5. Actuation

The electrothermal actuation behavior of the specimens was evaluated under a constant current (*I*) of 220 mA. All samples exhibited a clear and repeatable bending response, reaching a maximum tip deflection of 5.8 ± 0.6 mm, as shown in Figure 7.

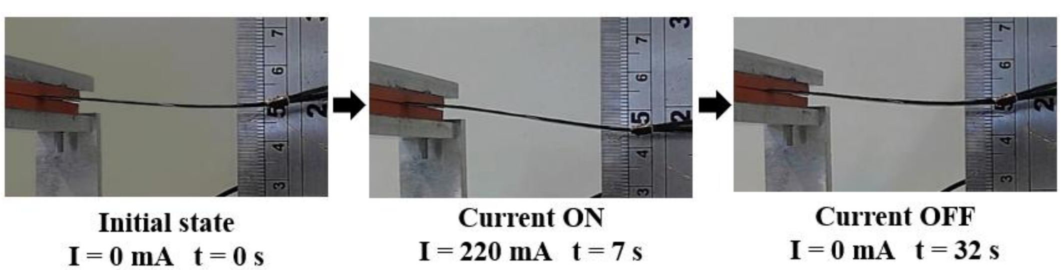

Figure 7. Electrothermal actuation of the FDM-manufactured specimen.

The actuation response of the cantilever beam was rapid during the initial stage, reaching the maximum deformation at elapsed time (t) ~ 7 s, followed by a gradual stabilization consistent with a transient thermal regime governed by Joule heating. Upon removal of the electrical current, the specimens exhibited a slower recovery, requiring ~ 25 s to return to 80–100% of their original position, reflecting the thermal dissipation and viscoelastic relaxation of the polymeric matrix. These results highlight the potential of FDM-fabricated CNT-based nanocomposites for electrothermally driven actuation, opening opportunities for their application in soft robotics and self-actuating structures.

4. Conclusions

The present study demonstrates that both filament composition, and architecture of FDM-manufactured parts critically determine the mechanical, electrical, and electromechanical performances of CNT-reinforced PLA and PLA–PHA filaments and FDM-manufactured parts. The main goal of the work was to achieve electrical conductivity above electrical percolation, without compromising mechanical properties. From a mechanical standpoint, the incorporation of CNTs led only to slight increases in elastic modulus with best performance around ~4 wt.% CNT, more emphatically in PLA–PHA systems. However, FDM-manufactured single-layer specimens showed a reduction in ductility and, in some cases, tensile strength. In terms of electrical behavior, CNT incorporation progressively improved electrical conductivity through the formation and densification of conductive pathways within the polymer matrix. PLA with 4 wt.% CNT filaments achieved an electrical conductivity of 5×10^{-5} S/cm, which is appropriate for piezoresistive sensing and actuating applications. FDM-manufactured single-layer specimens exhibited a decrease in electrical conductivity of 2–4 orders of magnitude compared to filaments. FDM-manufactured structures displayed enhanced piezoresistive sensitivity, driven by architectural and microstructural features introduced during printing. The electrothermal actuation results demonstrate that FDM-fabricated CNT-based multilayer structures can generate a stable and repeatable bending response under electrical stimulation.

References

[1] L. Remes, T.J. Massart, C. Fréderix, P. Hendrickx, P. Berke, CT-scan based mechanical finite element analysis of inter-filament voids in fused deposition modelling, Addit. Manuf. 114 (2025) 105032. https://doi.org/10.1016/j.addma.2025.105032.

[2] A.F. Wolstrup, J. Spangenberg, A. Yamamoto, A. Gleadall, G. Zsurzsan, Advances in 3D printed electromechanical sensors: Performance comparison, trends, and future directions, Addit. Manuf. 106 (2025) 104799. https://doi.org/10.1016/j.addma.2025.104799.

[3] J. Sharifi, G. Rizvi, H. Fayazfar, Toward Sustainable 3D-Printed Sensor: Green Fabrication of CNT-Enhanced PLA Nanocomposite via Solution Casting, Materials 17 (2024) 5782. https://doi.org/10.3390/ma17235782.

[4] L.J.B. Quaresma, D.S.C. Oliveira, R.S. Dias, K.C. Alves, L.G.D. de Barros, G. Pessin, A. Sinatora, W. Paraguassu, M.A.L. dos Reis, Anisotropic piezoresistive response of 3D-printed pressure sensor based on ABS/MWCNT nanocomposite, Sci. Rep. 14 (2024) 25297. https://doi.org/10.1038/s41598-024-76028-2.

[5] S. Lage-Rivera, A. Ares-Pernas, J.C. Becerra Permuy, A. Gosset, M.J. Abad, Enhancement of 3D Printability by FDM and Electrical Conductivity of PLA/MWCNT Filaments Using Lignin as Bio-Dispersant, Polymers 15 (2023) 999. https://doi.org/10.3390/polym15040999.

[6] R. Hashemi Sanatgar, A. Cayla, J. Guan, G. Chen, V. Nierstrasz, C. Campagne, Piezoresistive Properties of 3D-Printed Polylactic Acid (PLA) Nanocomposites, Polymers 14 (2022) 2981. https://doi.org/10.3390/polym14152981.

[7] A.R. Torrado Perez, D.A. Roberson, R.B. Wicker, Fracture surface analysis of 3D-printed tensile specimens of novel ABS-based materials, Journal of Failure Analysis and Prevention 14 (2014) 343–353. https://doi.org/10.1007/s11668-014-9803-9.

[8] G. Spinelli, R. Kotsilkova, E. Ivanov, I. Petrova-Doycheva, D. Menseidov, V. Georgiev, R. Di Maio, C. Silvestre, Effects of Filament Extrusion, 3D Printing and Hot-Pressing on Electrical and Tensile Properties of Poly(Lactic) Acid Composites Filled with Carbon Nanotubes and Graphene, Nanomaterials 10 (2019) 35. https://doi.org/10.3390/nano10010035.

[9] ColorFabb, Technical Datasheet color on demand, Belfeld, The Netherlands, 2018.

[10] ColorFabb, Technical Datasheet PLA/PHA, Belfeld, The Netherlands, 2023.

[11] F. Avilés, A. May-Pat, G. Canché-Escamilla, O. Rodríguez-Uicab, J.J. Ku-Herrera, S. Duarte-Aranda, J. Uribe-Calderon, P.I. Gonzalez-Chi, L. Arronche, V. La Saponara, Influence of carbon nanotube on the piezoresistive behavior of multiwall carbon nanotube/polymer composites, J. Intell. Mater. Syst. Struct. 27 (2016) 92–103. https://doi.org/10.1177/1045389X14560367.

[12] ASTM International, *ASTM D638-03: Standard Test Method for Tensile Properties of Plastics*, ASTM International, West Conshohocken, PA, USA, 2003.

[13] A. Bellini, S. Güçeri, Mechanical characterization of parts fabricated using fused deposition modeling, Rapid Prototyp. J. 9 (2003) 252–264. https://doi.org/10.1108/13552540310489631.

[14] D. Syrlybayev, B. Zharylkassyn, A. Seisekulova, M. Akhmetov, A. Perveen, D. Talamona, Optimisation of strength properties of FDM printed parts—A critical review, Polymers 13 (2021) 1587. https://doi.org/10.3390/polym13101587.

[15] J. Santo, P.K. Penumakala, R.B. Adusumalli, Mechanical and electrical properties of three-dimensional printed polylactic acid–graphene–carbon nanofiber composites, Polym. Compos. 42 (2021) 3231–3242. https://doi.org/10.1002/pc.26053.

[16] P.K. Penumakala, J. Santo, A. Thomas, A critical review on the fused deposition modeling of thermoplastic polymer composites, Compos. B Eng. 201 (2020) 108336. https://doi.org/10.1016/j.compositesb.2020.108336.

[17] M. Nowka, K. Ruge, L. Schulze, K. Hilbig, T. Vietor, Characterization of the Anisotropic Electrical Properties of Additively Manufactured Structures Made from Electrically Conductive Composites by Material Extrusion, Polymers 16 (2024) 2891. https://doi.org/10.3390/polym16202891.

[18] G. Spinelli, P. Lamberti, V. Tucci, L. Guadagno, L. Vertuccio, Damage monitoring of structural resins loaded with carbon fillers: Experimental and theoretical study, Nanomaterials 10 (2020) 434. https://doi.org/10.3390/nano10030434.

[19] F. Avilés, A.I. Oliva-Avilés, M. Cen-Puc, Piezoresistivity, Strain, and Damage Self-Sensing of Polymer Composites Filled with Carbon Nanostructures, Adv. Eng. Mater. 20 (2018) 1701159. https://doi.org/10.1002/adem.201701159.

[20] J.D. Banks, A. Emami, Carbon-Based Piezoresistive Polymer Nanocomposites by Extrusion Additive Manufacturing: Process, Material Design, and Current Progress, 3D Print. Addit. Manuf. 11 (2024) e548–e571. https://doi.org/10.1089/3dp.2022.0153.